Supplementary Information

Treasure Map for Nonmetallic Catalyst：Optimal Nitrogen and Fluorine Distribution of Biomass-Derived Carbon Materials for High-Performance Oxygen Reduction Catalysts

Yaling Zhao,‡[a] Yang Liu,‡[b] Ye Chen,[b] Xupo Liu,[b] Xiaoge Li,[c] Shuyan Gao*[ab]

[a]School of Chemistry and Chemical Engineering, Henan Normal University, Xinxiang, Henan 453007, P. R. China

[b]School of Materials Science and Engineering, Henan Normal University, Xinxiang, Henan 453007, P. R. China

[c]Key Laboratory of Mesoscopic Chemistry of MOE, School of Chemistry and Chemical Engineering, Nanjing University, Nanjing, Jiangsu 210023, P. R. China.

*Corresponding authors: shuyangao@htu.cn

‡Y. Zhao and Y. Liu contribute equally to this work.

EXPERIMENTAL SECTION

Materials:

All chemicals were of analytical grade and used directly as received. Zinc chloride ($ZnCl_2$), ammonium hydroxide ($NH_3 \cdot H_2O$), ammonium fluoride (NH_4F), and hydrochloric acid (HCl) were obtained from Alfa Aesar. Nearly 30 kinds of natural biomass were purchased from a vegetable market in Xinxiang and washed for further use.

Preparation of N, F dual-doped porous carbon materials:

The washed alfalfa was dried and smashed by a pulverizer. 1 g of alfalfa powder and 0.37 g of NH_4F (0.01 mol) were mixed well in a mortar, then carbonized in N_2 atmosphere at 500 °C for 2 h, later naturally cooled to room temperature. 0.022 mol of $NH_3 \cdot H_2O$ was rapidly dropped into a $ZnCl_2$ aqueous solution (containing 0.022 mol of $ZnCl_2$) to obtain a mixed activator suspension liquid consisting of $ZnCl_2$ and $Zn(OH)_2$. The beforehand carbonized product was mixed with above suspension liquid uniformly and dried, carbonized for 2 h in N_2 flow at 900 ^oC, subsequently immersing in 2 mol L^{-1} HCl overnight, and then washed with water to neutral to obtain the N, F co-doped porous carbon material (NF-PC). The NF-PCs obtained with alfalfa as precursor are denoted as NF-x. For comparison, the control samples of NF-3.31, NF-4.27, NF-4.84, NF-5.58, NF-6.44 and NF-7.19 were prepared using the same synthesis method except for different molar dosages of NH_4F, which were 0.001, 0.005, 0.01, 0.02, 0.03 and 0.04 mol, respectively. The others NF-PCs obtained from the additional 26 biomass species are denoted as NF-y. Both x and y represent the total N, F contents incorporated in in site NF-PCs.

Preparation of working electrode:

The glassy carbon electrode (GC, diameter = 3/5 mm) was polished with an alumina (0.05 μm) polishing solution. 1 mg of sample, 20 μL of Nafion ethanol solution and 100 μL of ultrapure water, were mixed well through a ultrasonic treatment for 30 minutes to obtain the uniform ink-like liquid. 5/12 μL of above ink-like liquid was dropped on the GC (diameter = 3/5 mm), then dried naturally for further use. The final loading mass were 0.59 and 0.51 mg cm^{-2} for 3 and 5 mm GC, respectively.

Electrochemical measurements:

The rotating ring-disk/disk electrode test (RRDE, 5 mm in diameter) and cyclic voltammetry (CV, 3 mm) were performed in 0.1/1 mol L^{-1} KOH solution saturated with N_2 or O_2 through a CHI 660E/760E electrochemical workstation at room temperature. A platinum sheet (1 cm^2), a glassy carbon electrode coated with the catalyst, and a reversible hydrogen electrode (RHE) were used as the counter, working and reference electrode, respectively. Except for the 50 mV s^{-1} of scan rates for methanol resistance tests, the scan rates were 10 mV s^{-1} for the other CV tests. The scan potential ranges were 0.07 ~ 1.06 V and 0.8 ~ 1.8 V for ORR and OER measurements by using RRDE/RDE system. The scan rates were 10 mV s^{-1} and electrode rotation speeds were 1600 rpm for both RRDE and RDE measurements. The H_2O_2 yield and electron transfer number during ORR were acquired by the following formulas (Equation 1 & 2):

$$n = 4I_d/(I_d + I_r/N) \quad \textbf{(1)}$$

$$H_2O_2\% = 200I_r/(NI_d + I_r) \quad \textbf{(2)}$$

where n is the electron transfer number and $H_2O_2\%$ is the hydrogen peroxide yield during ORR process, I_d is the disk current, I_r is the ring current, N represents the current collection efficiency of the platinum ring and $N = 0.37$.

Rechargeable Zn−Air Battery

The as-prepared catalyst and Pt/C was treated to an ink status as described in above electrochemical measurements section. The catalyst ink was dropped on the carbon paper and dried to obtain an air−cathode diffusion layer. The loading mass was 1.0 mg cm^{-2} for metal-free porous carbon material and 1.0 mg cm^{-2} for Pt/C. As a comparison, the Pt/C and IrO_2 ink with a loading mass of 1.0 and 1.0 mg cm^{-2} were employed as the air−cathode diffusion layer for another ZAB. A zinc plate was as the another anode and 6 M KOH solution containing 0.2 M $Zn(Ac)_2{\cdot}2H_2O$ was employed as the electrolyte. The charge-discharge curves were collected by CHI 760E electrochemical workstation. The galvanostatic charge−discharge measurements were carried out by chronopotentiometry test system.

Characterization:

Microscopic morphologies of all the samples were investigated by the field emission scanning electron microscopy (FE-SEM, Zeiss Supra 40, Japan) and transmission electron microscopy (TEM, JEOL JEM-2100, Japan). The porous nature was determined via the density functional theory (DFT) method by analyzing the N_2 adsorption-desorption isotherms, which were recorded at 77 K using a Micromeritics ASAP 2020 apparatus. The Raman and X-ray diffraction (XRD) patterns were collected using a Renishaw Spectroscopy with a 514 nm excitation laser and a Bruker-D8 instrument with Cu radiation, respectively. The elemental compositions were qualitatively and quantitatively analyzed by the X-ray

photoelectron spectroscopy (XPS, ESCALAB 250, America) measurement. The water contact angle (CA) test was performed using the contact angle meter (KRüSS DSA25, Germany).

Discussion

The influence of heteroatom source (NH_4F) and porogen ($ZnCl_2$ and $Zn(OH)_2$) on the composition and pore structure of carbon materials has been studied. Except for NF-4.84 (alfalfa mixed with both NH_4F and porogens were carbonized), the control samples of C (only alfalfa was carbonized), C-NF (alfalfa mixed with NH_4F were carbonized) and C-Zn (alfalfa mixed with porogens were carbonized) were prepared. The SEM images shown in **Fig. S17a-17d** indicate that the addition of both NH_4F and porogens is resulted in abundant nanoscale pores in carbon material. The XPS spectra (**Fig. S17e**, **Table S1**) of C-NF and NF-4.84 demonstrate the successful incorporation of N and F into carbon matrix when using NH_4F as heteroatom source. According to N_2 adsorption/desorption isotherms (**Fig. S17f)** and pore size distributions (**Fig. S17g**), obviously, NF-4.84 possesses the largest specific surface area (Table S1) and most pore amount among C, C-NF, C-Zn and NF-4.84. XRD (**Fig. S17h)** and Raman (**Fig. S17i**) results present the coexistence of disorder nature and partial graphitization in these carbon materials. Moreover, the electrochemical measurement results including CV (**Fig. S17j**) and RRDE curves (**Fig. S17k**) manifest that NF-4.84 exhibits the most positive peak potential (Table S1) and half wave potential, as well as the largest peak current density and limiting current density. Briefly, the above information reveals that NF-4.84 sample with both N, F heteroatoms and large specific surface area exhibits the remarkable ORR performance (**Fig. S17j, k**).

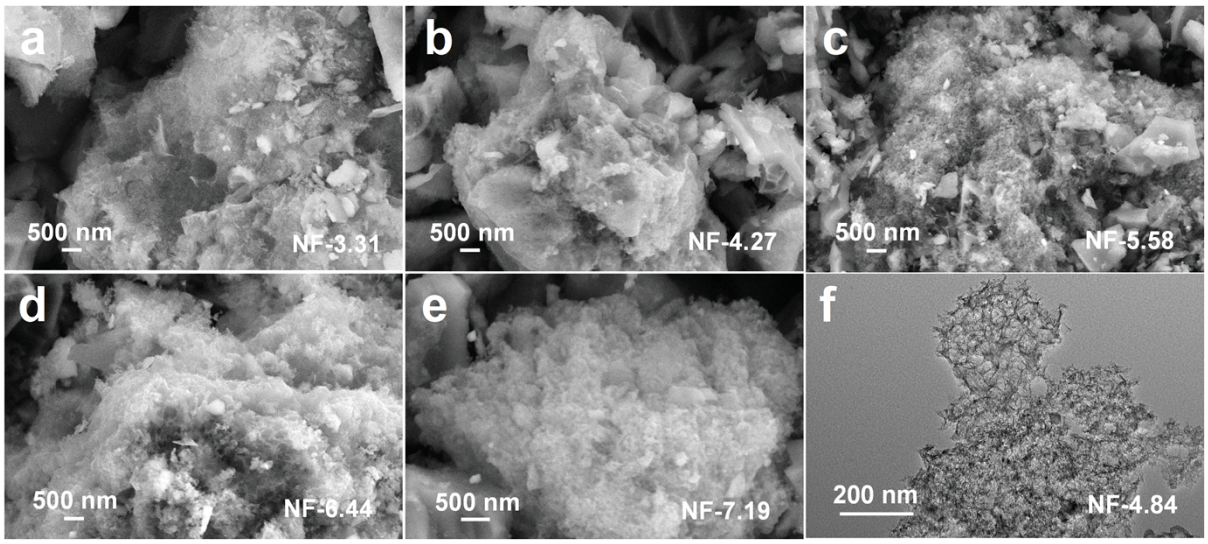

Fig. S1 (a-e) FE-SEM images NF-x. (f) TEM image of NF-4.84.

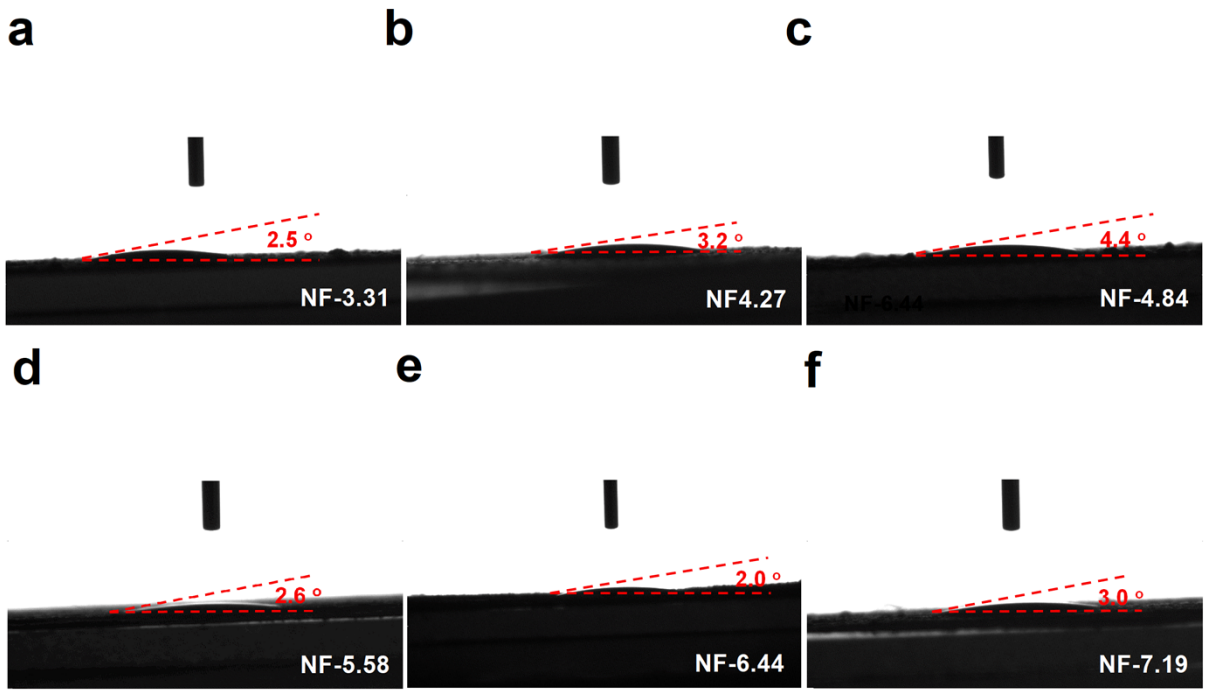

Fig. S2 CA images for NF-x.

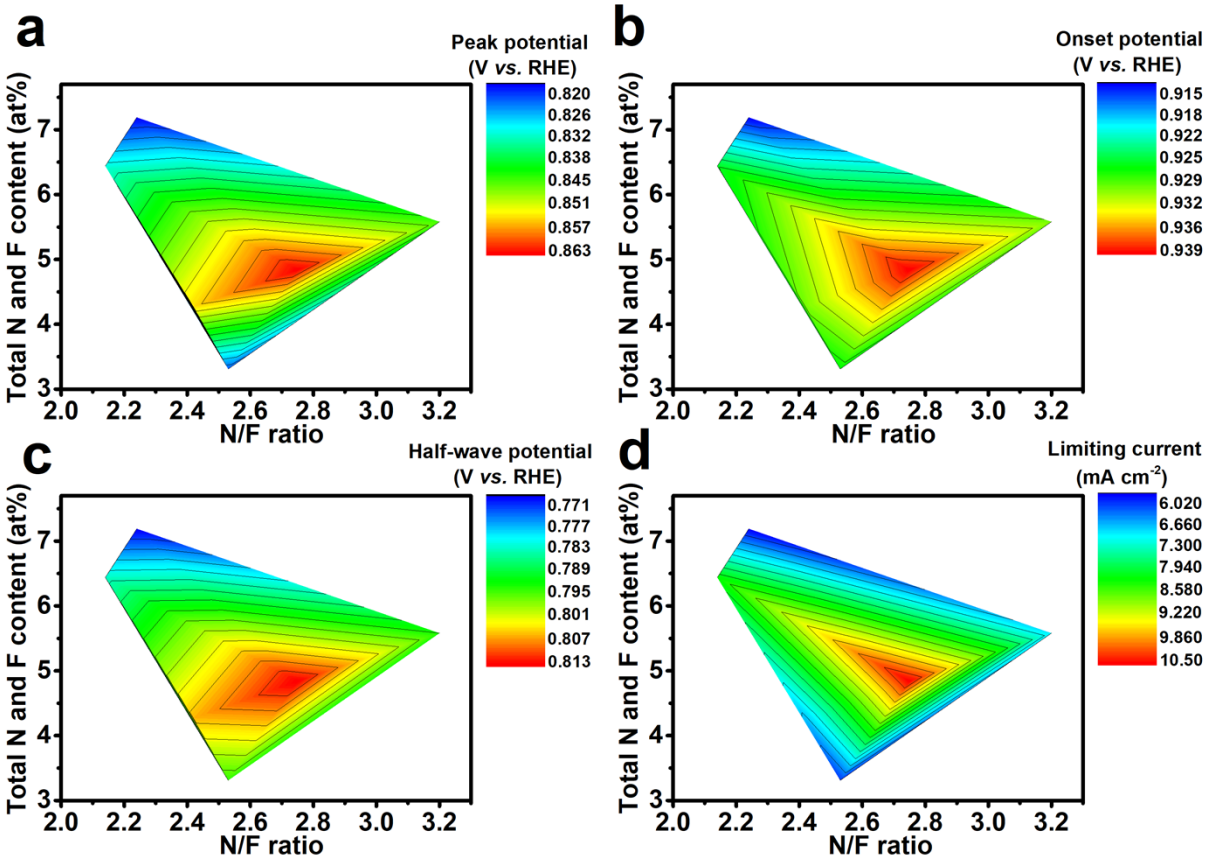

Fig. S3 Linearized activity volcano for (a) peak potential, (b) onset potential, (c) half-wave potential and (d) limiting current density as the function of total N, F content and N/F ratio based on NS-x. Dark red indicates maximum ORR activity.

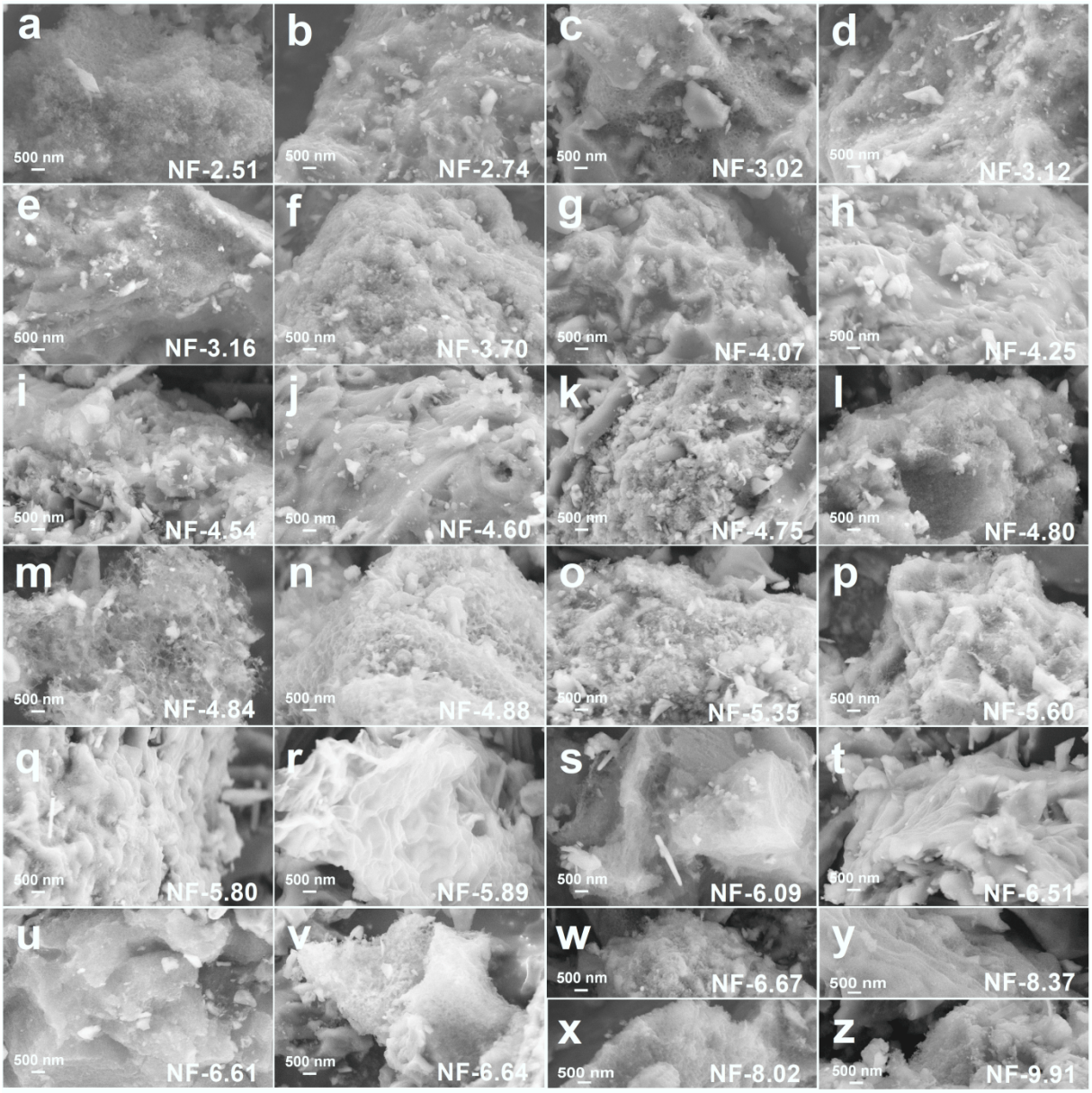

Fig. S4 The SEM images for NF-y derived from (a) cantaloupe peel, (b) pomegranate peel, (c) bark, (d) longan shell, (e) white beech mushroom, (f) oil bran, (g) apricot flowers, (h) radish leaves, (i) corn stigmas, (j) winter melon peel, (k) durian peel, (l) willow leaves, (m) alfalfa, (n) banana peel, (o) radish peel, (p) leek moss, (q) dandelion leaves, (r) long bean, (s) sweet potato stems, (t) orange peel, (u) soybean curb residue, (v) firmiana simplex flowers, (w) sweet potato leaves, (x) wheat stalk, (y) solidago, (z) pepper leaves.

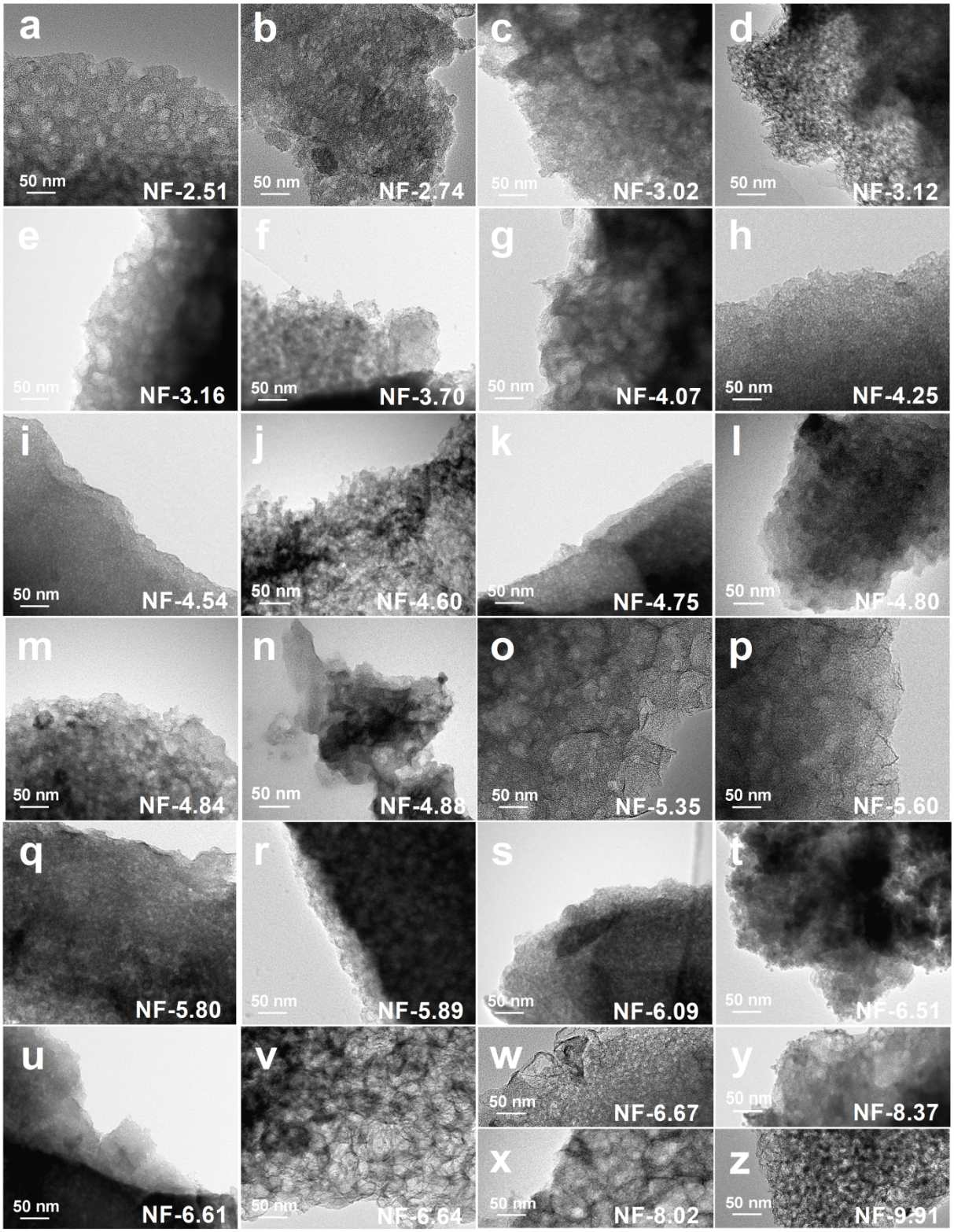

Fig. S5 The TEM images for NF-y derived from (a) cantaloupe peel, (b) pomegranate peel, (c) bark, (d) longan shell, (e) white beech mushroom, (f) oil bran, (g) apricot flowers, (h) radish leaves, (i) corn stigmas, (j) winter melon peel, (k) durian peel, (l) willow leaves, (m) alfalfa, (n) banana peel, (o) radish peel, (p) leek moss, (q) dandelion leaves, (r) long bean, (s) sweet potato stems, (t) orange peel, (u) soybean curb residue, (v) firmiana simplex flowers, (w) sweet potato leaves, (x) wheat stalk, (y) solidago, (z) pepper leaves.

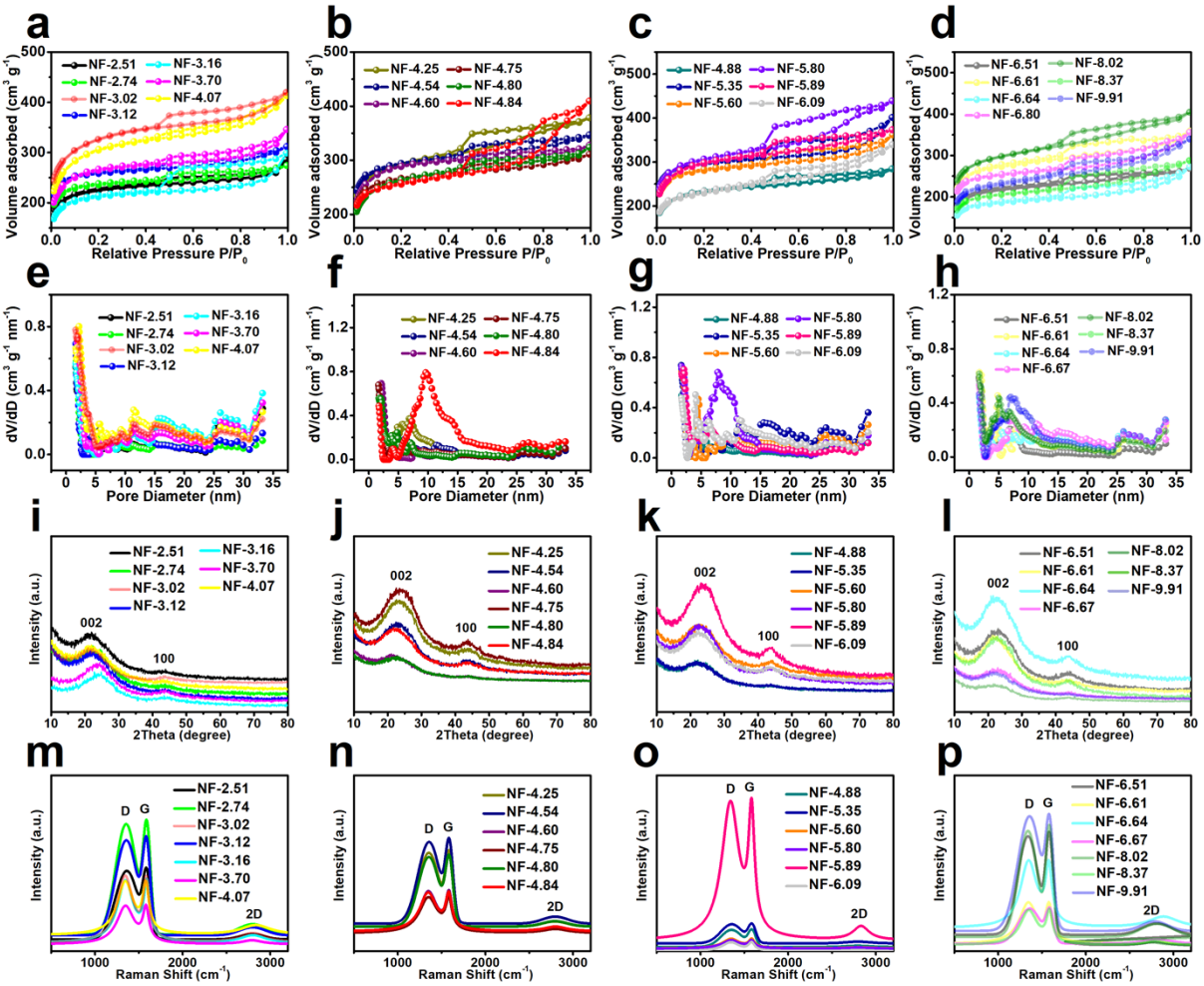

Fig. S6 (a-d) N_2 adsorption/desorption isotherms, (e-h) pore size distributions, (i-l) XRD and (m-p) Raman patterns for NF-y derived from cantaloupe peel, pomegranate peel , bark, longan shell, white beech mushroom, oil bran, apricot flowers, radish leaves corn stigmas, winter melon peel, durian peel, willow leaves, alfalfa, banana peel, radish peel, leek moss, dandelion leaves, long bean, sweet potato stems, orange peel, soybean curb residue, firmiana simplex flowers, sweet potato leaves, wheat stalk, solidago, pepper leaves.

Fig. S7 Water contact images for NF-y derived from (a) cantaloupe peel, (b) pomegranate peel, (c) bark, (d) longan shell, (e) white beech mushroom, (f) oil bran, (g) apricot flowers, (h) radish leaves, (i) corn stigmas, (j) winter melon peel, (k) durian peel, (l) willow leaves, (m) alfalfa, (n) banana peel, (o) radish peel, (p) leek moss, (q) dandelion leaves, (r) long bean, (s) sweet potato stems, (t) orange peel, (u) soybean curb residue, (v) firmiana simplex flowers, (w) sweet potato leaves, (x) wheat stalk, (y) solidago, (z) pepper leaves.

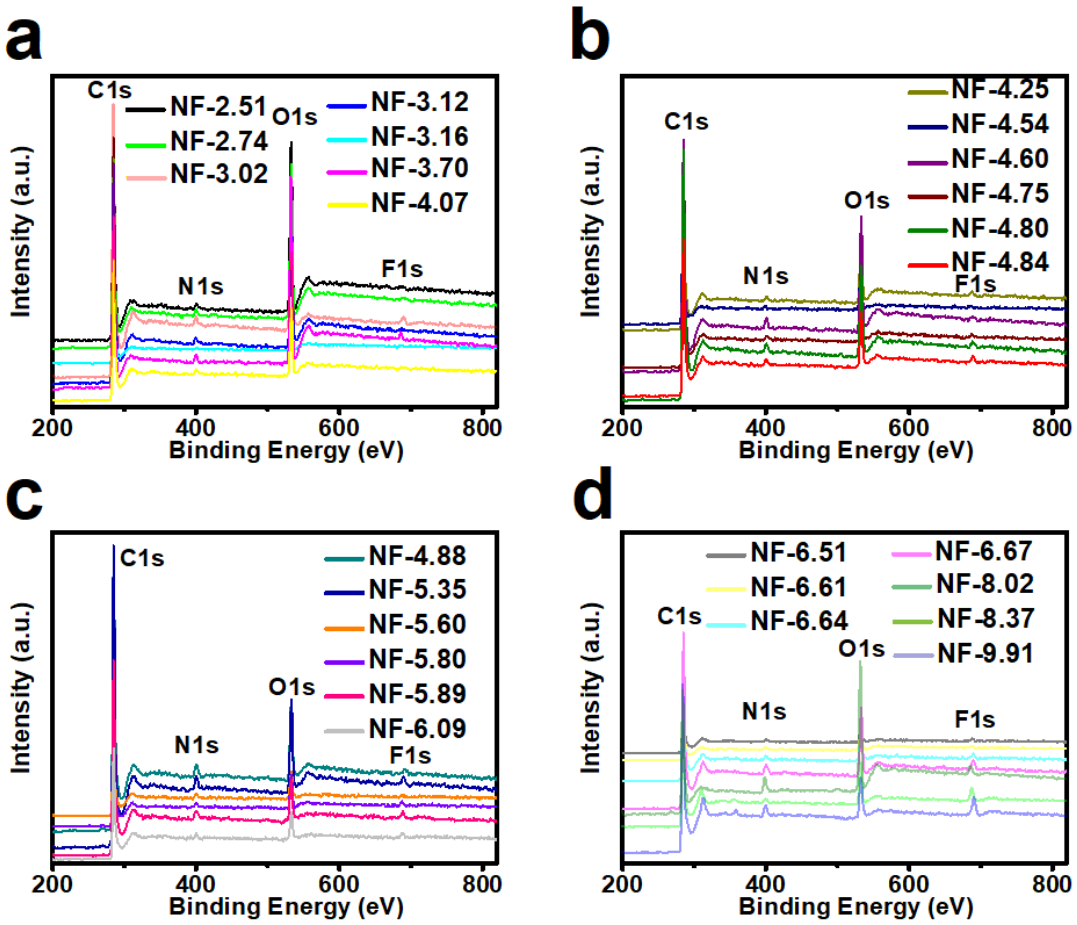

Fig. S8 XPS full spectra for NF-y derived from derived from cantaloupe peel, pomegranate peel , bark, longan shell, white beech mushroom, oil bran, apricot flowers, radish leaves corn stigmas, winter melon peel, durian peel, willow leaves, alfalfa, banana peel, radish peel, leek moss, dandelion leaves, long bean, sweet potato stems, orange peel, soybean curb residue, firmiana simplex flowers, sweet potato leaves, wheat stalk, solidago, pepper leaves.

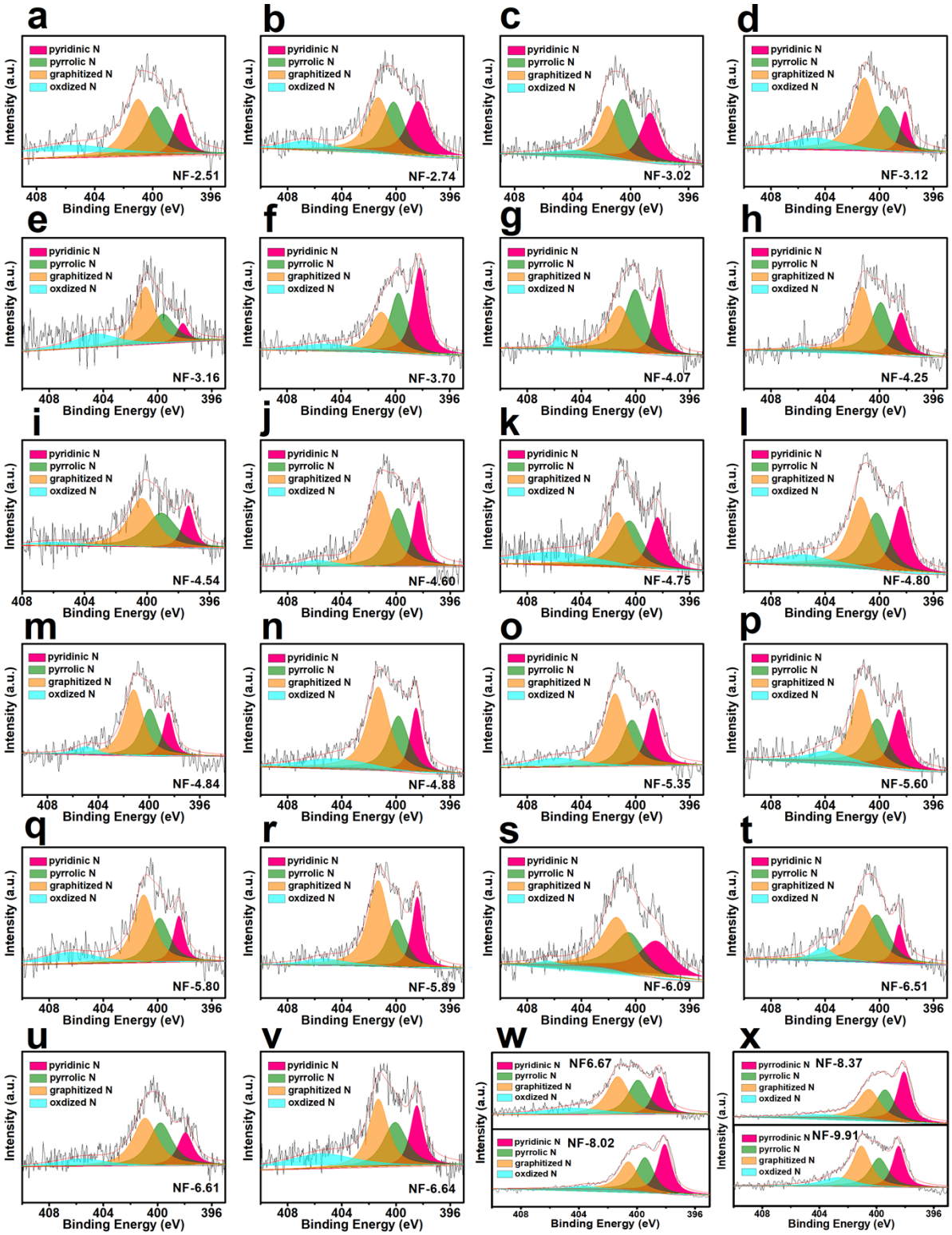

Fig. S9 High resolution N1s spectra for NF-y derived from (a) cantaloupe peel, (b) pomegranate peel, (c) bark, (d) longan shell, (e) white beech mushroom, (f) oil bran, (g) apricot flowers, (h) radish leaves, (i) corn stigmas, (j) winter melon peel, (k) durian peel, (l) willow leaves, (m) alfalfa, (n) banana peel, (o) radish peel, (p) leek moss, (q) dandelion leaves, (r) long bean, (s) sweet potato stems, (t) orange peel, (u) soybean curb residue, (v) firmiana simplex flowers, (w) sweet potato leaves and wheat stalk, (x) solidago and pepper leaves.

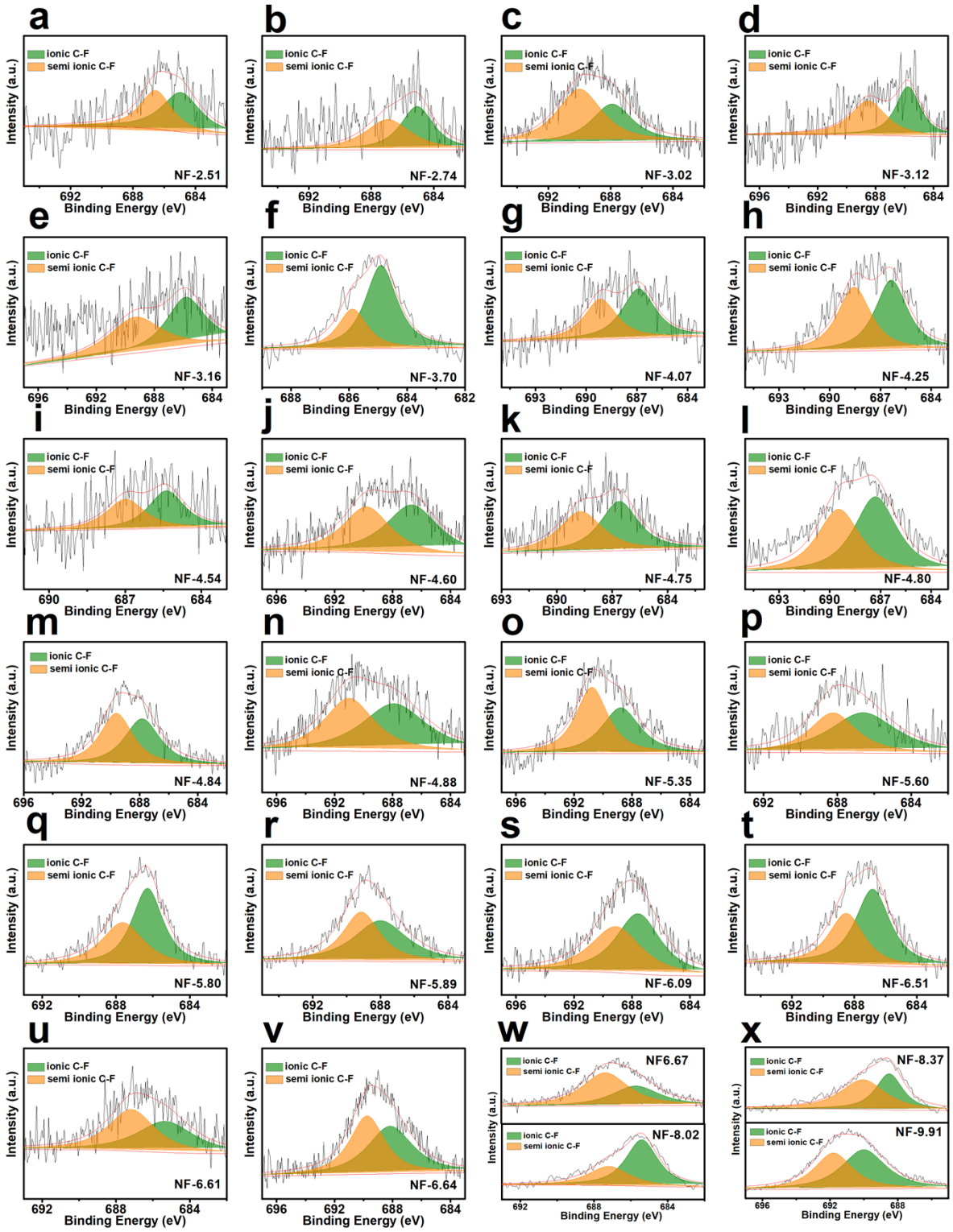

Fig. S10 High resolution F1s spectra for NF-y derived from (a) cantaloupe peel, (b) pomegranate peel, (c) bark, (d) longan shell, (e) white beech mushroom, (f) oil bran, (g) apricot flowers, (h) radish leaves, (i) corn stigmas, (j) winter melon peel, (k) durian peel, (l) willow leaves, (m) alfalfa, (n) banana peel, (o) radish peel, (p) leek moss, (q) dandelion leaves, (r) long bean, (s) sweet potato stems, (t) orange peel, (u) soybean curb residue, (v) firmiana simplex flowers, (w) sweet potato leaves and wheat stalk, (x) solidago and pepper leaves.

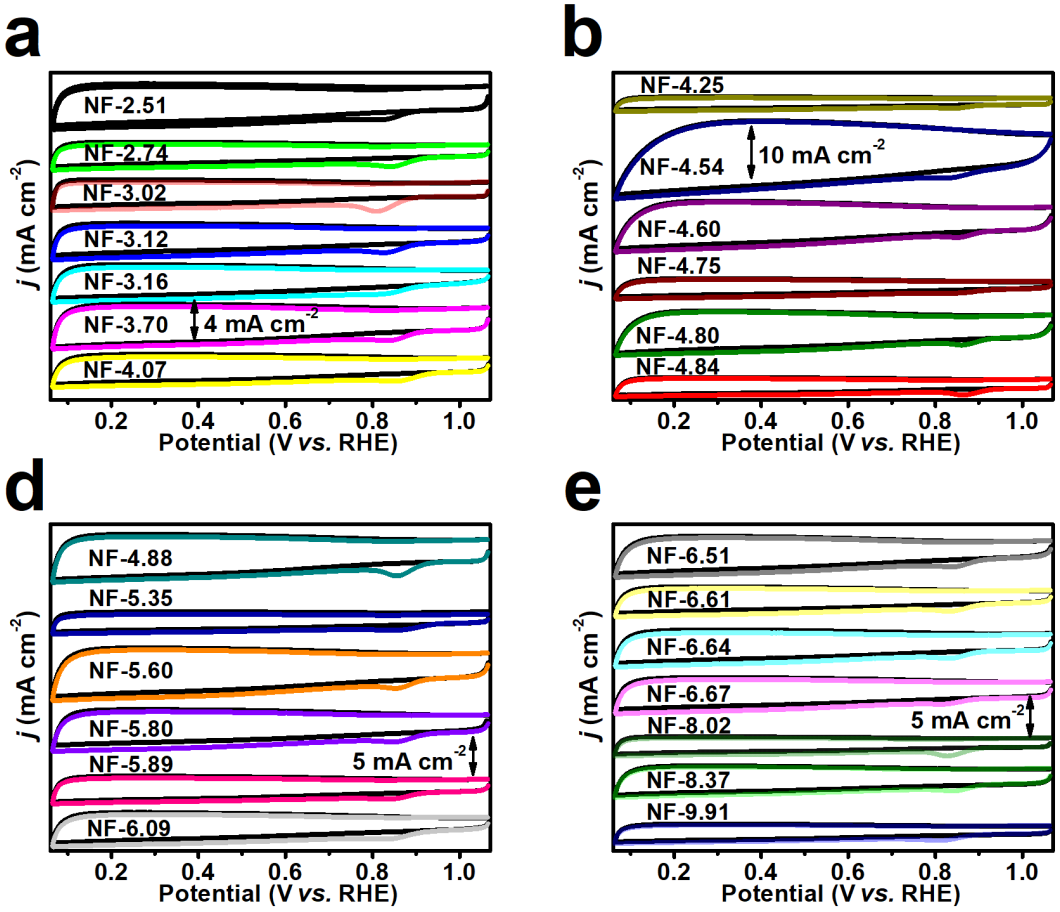

Fig. S11 CV curves (the as-obtained black/colored lines at N_2/O_2-saturated electrolyte) for NF-y derived from derived from cantaloupe peel, pomegranate peel , bark, longan shell, white beech mushroom, oil bran, apricot flowers, radish leaves corn stigmas, winter melon peel, durian peel, willow leaves, alfalfa, banana peel, radish peel, leek moss, dandelion leaves, long bean, sweet potato stems, orange peel, soybean curb residue, firmiana simplex flowers, sweet potato leaves, wheat stalk, solidago, pepper leaves.

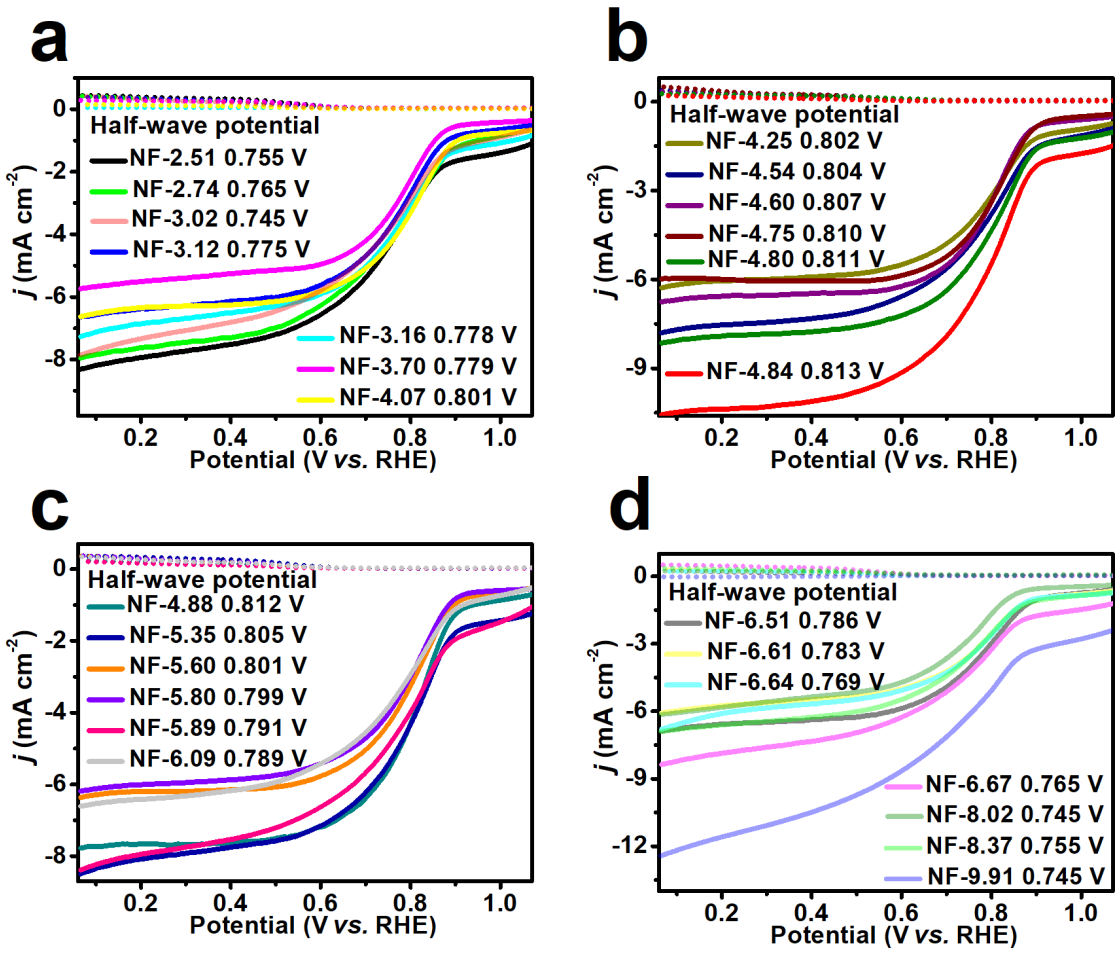

Fig. S12 RRDE curves (the solid/dotted lines for disk/ring current density) for NF-y derived from cantaloupe peel, pomegranate peel , bark, longan shell, white beech mushroom, oil bran, apricot flowers, radish leaves corn stigmas, winter melon peel, durian peel, willow leaves, alfalfa, banana peel, radish peel, leek moss, dandelion leaves, long bean, sweet potato stems, orange peel, soybean curb residue, firmiana simplex flowers, sweet potato leaves, wheat stalk, solidago, pepper leaves.

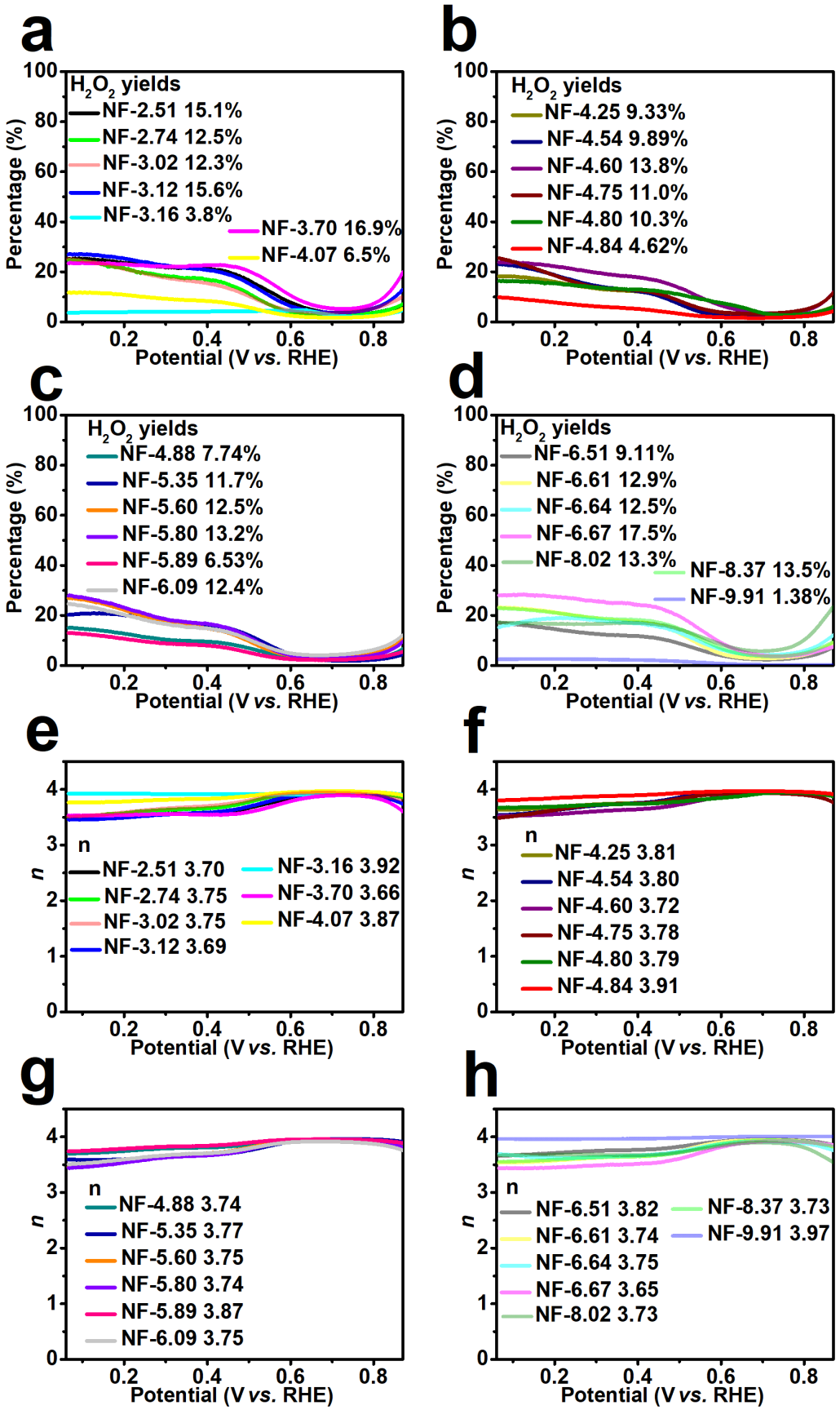

Fig. S13 (a-d) H_2O_2% yields, (e-h) electron transfer number for NF-y.

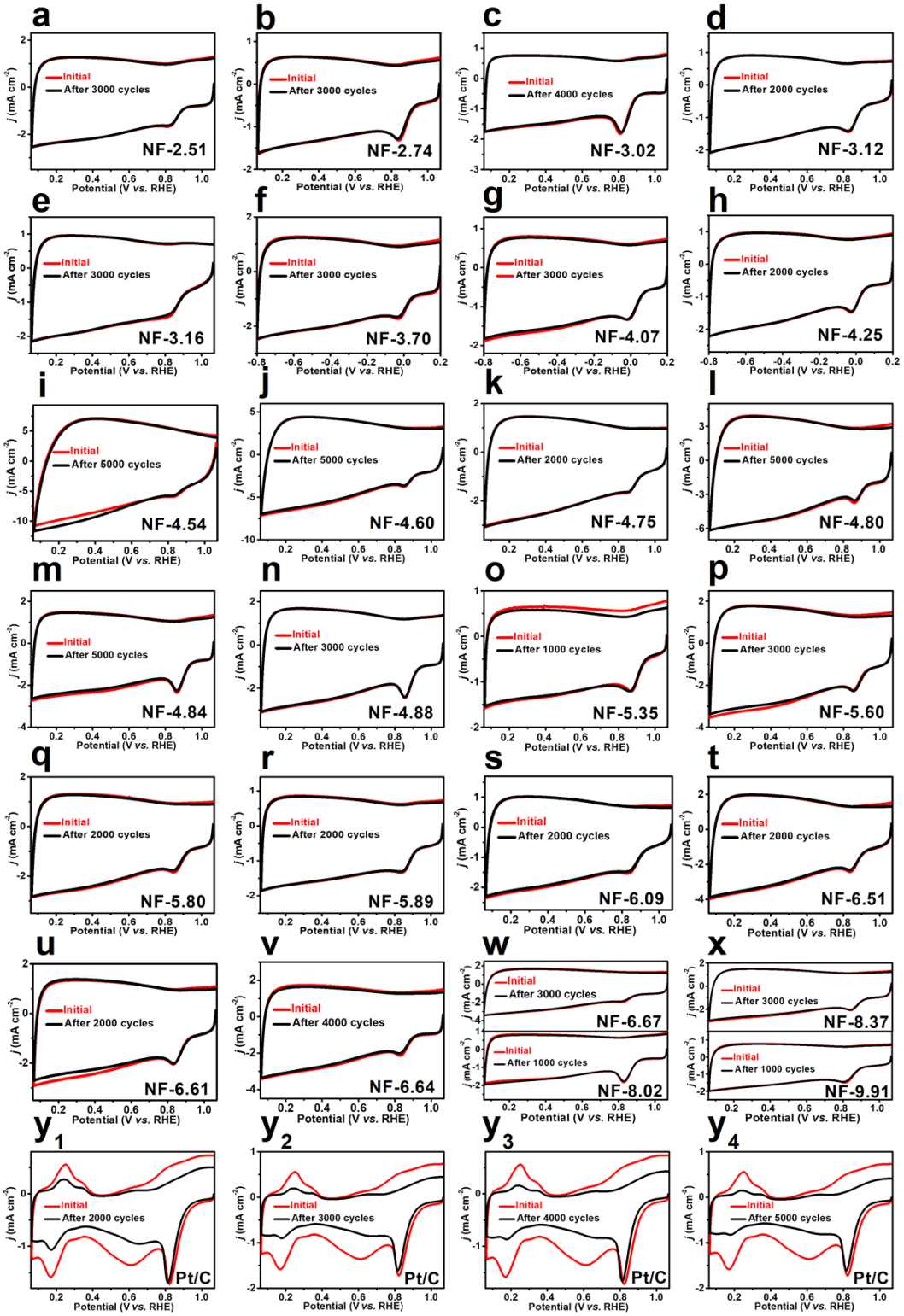

Fig. S14 Stability tests for NF-y from (a) cantaloupe peel, (b) pomegranate peel, (c) bark, (d) longan shell, (e) white beech mushroom, (f) oil bran, (g) apricot flowers, (h) radish leaves, (i) corn stigmas, (j) winter melon peel, (k) durian peel, (l) willow leaves, (m) alfalfa, (n) banana peel, (o) radish peel, (p) leek moss, (q) dandelion leaves, (r) long bean, (s) sweet potato stems, (t) orange peel, (u) soybean curb residue, (v) firmiana simplex flowers, (w) sweet potato leaves and wheat stalk, (x) solidago and pepper leaves, (y) Pt/C.

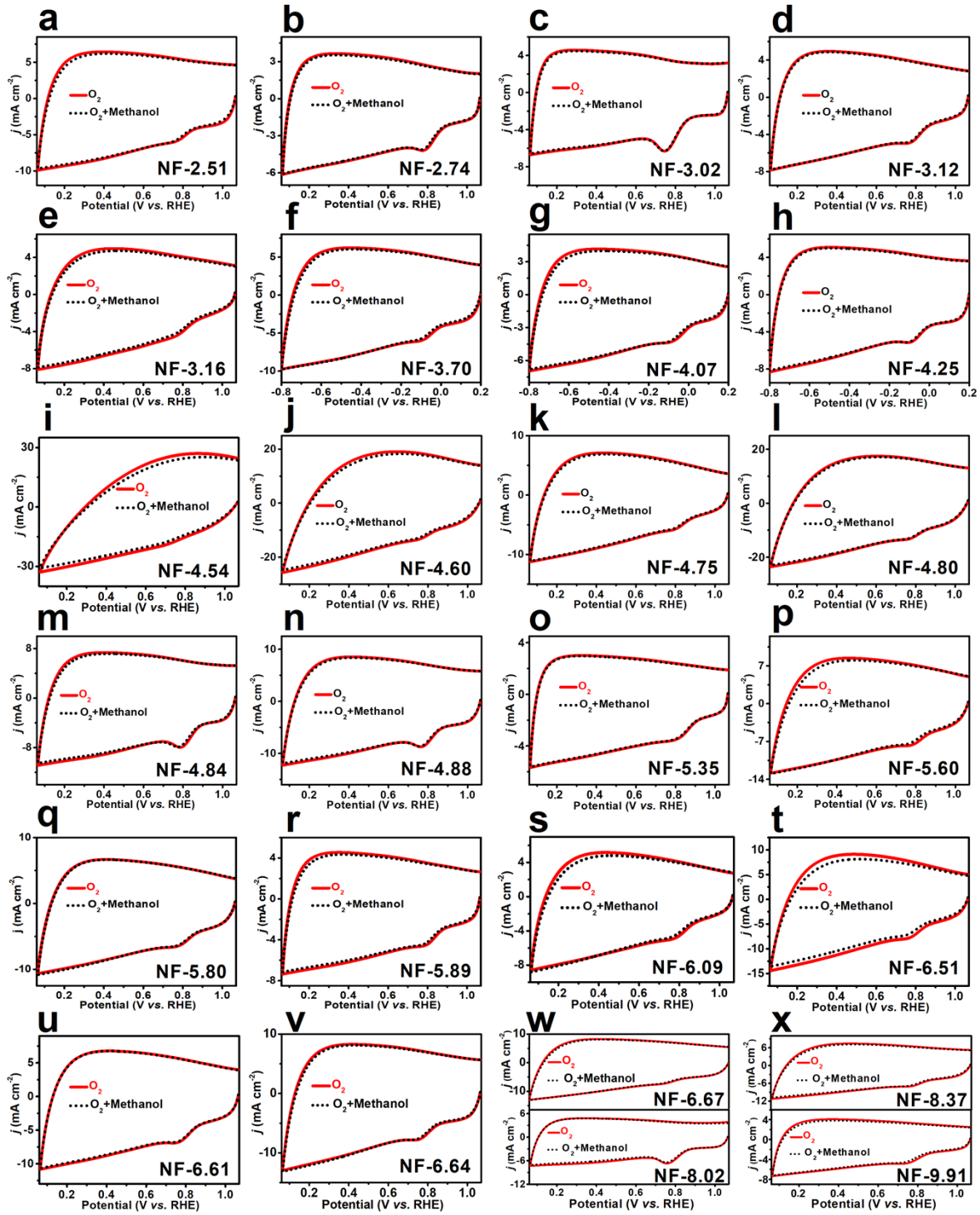

Fig. S15 Methanol tolerance tests for NF-y derived from (a) cantaloupe peel, (b) pomegranate peel, (c) bark, (d) longan shell, (e) white beech mushroom, (f) oil bran, (g) apricot flowers, (h) radish leaves, (i) corn stigmas, (j) winter melon peel, (k) durian peel, (l) willow leaves, (m) alfalfa, (n) banana peel, (o) radish peel, (p) leek moss, (q) dandelion leaves, (r) long bean, (s) sweet potato stems, (t) orange peel, (u) soybean curb residue, (v) firmiana simplex flowers, (w) sweet potato leaves and wheat stalk, (x) solidago and pepper leaves.

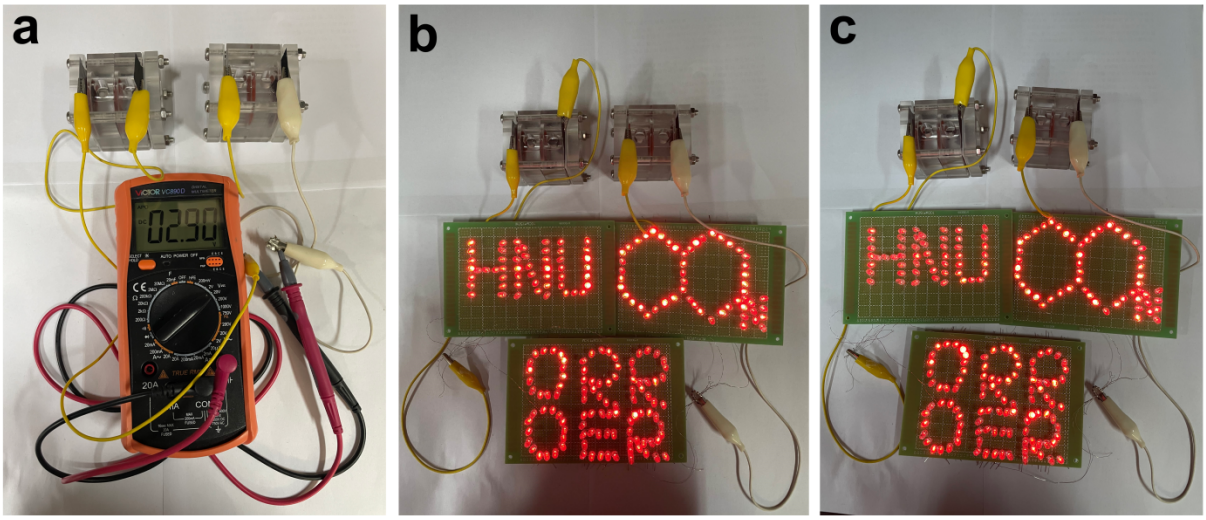

Fig. S16 (a) Photograph of two series-connected ZABs with a measured open-circuit of 2.90 V, photographs for 210 LEDs driven by two ZABs (b) before and (c) after 24 hours.

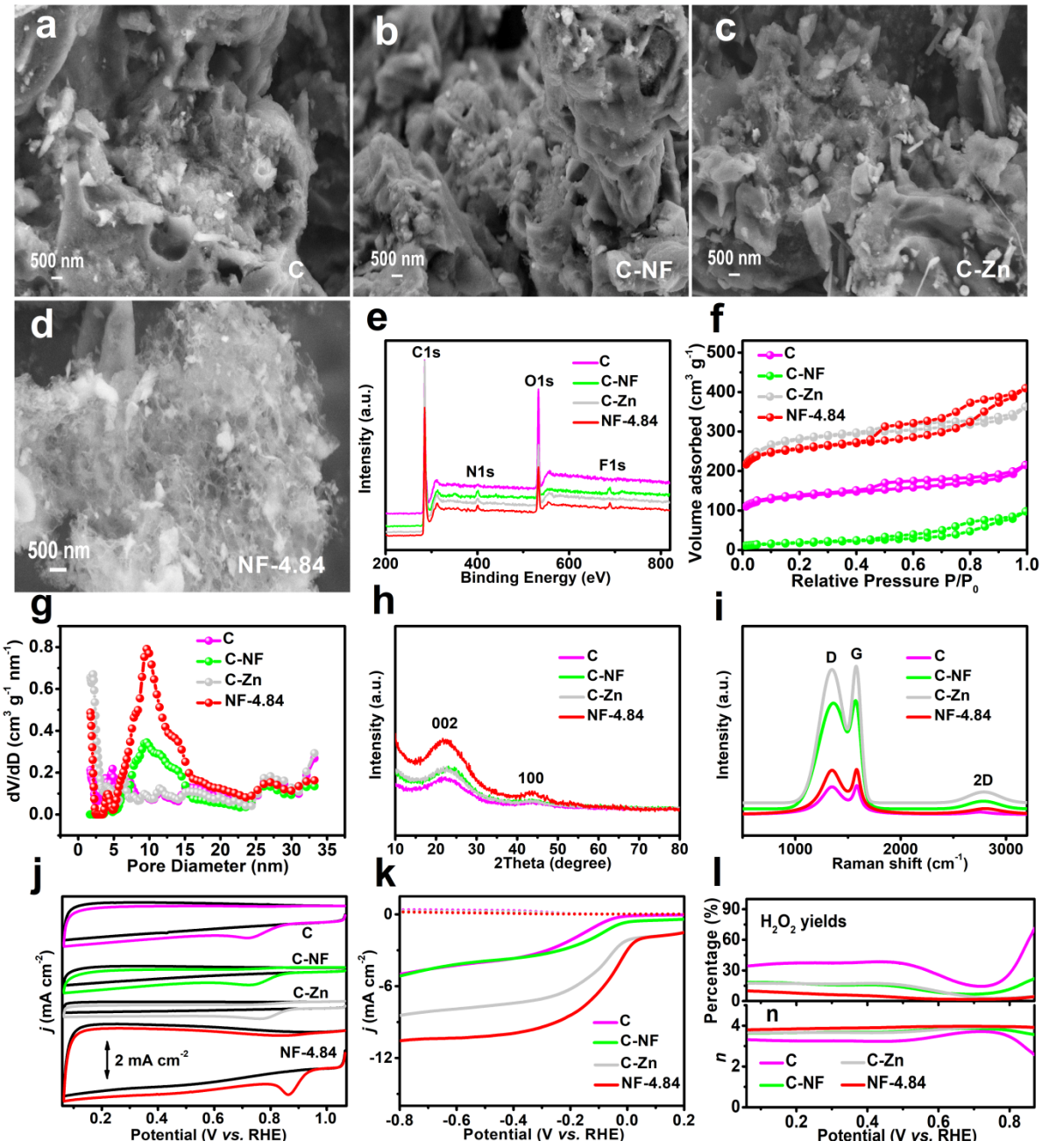

Fig. S17 (a-d) SEM images, (e) XPS full spectra, (f) N_2 adsorption-desorption isotherms, (g) pore size distributions, (h) XRD patterns, (i) Raman spectra, (j) CV curves, (k) RRDE curves, H_2O_2 yields and (l) *n* for C, C-NF, C-Zn and NF-4.8, respectively.

Table S1 Structural and electrocatalytic information for samples derived from alfalfa.

Sample	S_{BET} [m^2 g^{-1}][a)]	N content [at. %][b)]	F content [at. %][c)]	N and F content [at.%][d)]	N /F[e)]	E_{peak} [V][f)]	E_{onset} [V][g)]	$E_{half\text{-}wave}$ [V][h)]	$J_{limiting}$ [mA cm^{-2}][i)]
NF-3.31	1350	2.58	0.73	3.31	2.53	0.821	0.926	0.793	-6.0
NF-4.27	1452	3.02	1.25	4.27	2.42	0.853	0.929	0.805	-6.6
NF-4.84	1384	3.55	1.29	4.84	2.75	0.863	0.943	0.806	-10.5
NF-5.58	1400	4.25	1.33	5.58	3.20	0.843	0.929	0.792	-6.8
NF-6.44	1487	4.39	2.05	6.44	2.14	0.830	0.925	0.782	-8.1
NF-7.19	1395	4.97	2.22	7.19	2.24	0.817	0.913	0.768	-5.7
Pt/C	—	—	—	—	—	0.830	0.963	0.805	-6.6
C	662	1.63	—	—	—	0.723	0.845	0.635	-5.0
C-NF	75	4.14	1.82	5.96	2.27	0.736	0.871	0.695	-5.2
C-Zn	1251	2.97	—	—	—	0.778	0.902	0.778	-8.4

[a)]BET specific surface area; [b)]Nitrogen content; [c)]Flourine content; [d)]Total nitrogen and flourine content; [e)]The ratio of N to F content; [f)]Peak potential; [g)]Onset potential; [h)]Half-wave potential; [i)]Diffusion-limited current.

Table S2 Structure information of N, F dual-doped porous carbon materials derived from different biomass precursors.

Biomass	Sample	S_{BET} [$m^2\ g^{-1}$][a)]	N content [at. %][b)]	F content [at. %][c)]	N and F content [at.%][d)]	N /F[e)]	I_D/I_G[f)]	CA (°)[g)]
cantaloupe peel	NF-2.51	1030	1.84	0.67	2.51	2.75	1.21	1.5
pomegranate peel	NF-2.74	1105	2.24	0.5	2.74	4.48	1.12	3.0
bark	NF-3.02	1397	1.81	1.21	3.02	1.50	1.16	3.9
longan shell	NF-3.12	1311	2.47	0.65	3.12	3.8	1.17	3.2
white beech mushroom	NF-3.16	1001	2.26	0.9	3.16	2.51	1.18	3.3
oil bran	NF-3.70	1180	2.62	1.08	3.7	2.43	1.19	5.0
apricot flowers	NF-4.07	1284	3.28	0.79	4.07	4.15	1.17	4.1
radish leaves	NF-4.25	1391	2.92	1.33	4.25	2.2	1.16	2.1
corn stigmas	NF-4.54	1389	3.72	0.82	4.54	4.54	1.18	5.0
winter melon peel	NF-4.60	1306	3.74	0.86	4.6	4.35	1.19	2.5
durian peel	NF-4.75	1269	3.51	1.24	4.75	2.83	1.13	1.3
willow leaves	NF-4.80	1207	3.71	1.09	4.80	3.40	1.15	3.0
alfalfa	NF-4.84	1384	3.55	1.29	4.84	2.75	1.19	4.4
banana peel	NF-4.88	1088	3.75	1.13	4.88	3.31	1.14	3.8
radish peel	NF-5.35	1398	4.11	1.24	5.35	3.31	1.16	4.2
leek moss	NF-5.60	1337	4.4	1.2	5.6	3.67	1.18	5.0
dandelion leaves	NF-5.80	1395	3.85	1.95	5.8	1.97	1.20	3.6
long bean	NF-5.89	1322	4.41	1.48	5.89	2.98	1.18	2.5
sweet potato stems	NF-6.09	1102	3.92	2.17	6.09	1.81	1.18	3.5
orange peel	NF-6.51	1023	4.24	2.27	6.51	1.88	1.18	1.0
soybean curb residue	NF-6.61	1241	5.26	1.35	6.61	2.65	1.20	1.2
firmiana simplex flowers	NF-6.64	1007	4.56	2.08	6.64	2.19	1.20	2.4
sweet potato leaves	NF-6.67	1366	4.35	2.32	6.67	1.88	1.20	3.2
wheat stalk	NF-8.02	1388	6.51	1.51	8.02	4.31	1.18	3.4
solidago	NF-8.37	1039	4.5	3.87	8.37	1.16	1.19	3.2
pepper leaves	NF-9.91	1154	5.42	4.49	9.91	1.21	1.21	4.0

[a)]BET specific surface area; [b)]Nitrogen content; [c)]Flourine content; [d)]Total nitrogen and flourine content; [e)]The ratio of N to F content; [f)]I_D/I_G value;[g)]water contact angle.

Table S3 Electrocatalytic performances of N, F dual-doped porous carbon materials derived from different biomass precursors.

Biomass	Biomass	E_{peak} [V][a)]	J_{peak} [mA cm^{-2}][b)]	$E_{half\text{-}wave}$ [V][c)]	E_{onset} [V][d)]	$J_{limiting}$ [mA cm^{-2}][e)]
cantaloupe peel	NF-2.51	0.823	-1.72	0.755	0.916	-8.3
pomegranate peel	NF-2.74	0.842	-1.36	0.765	0.917	-8.0
bark	NF-3.02	0.810	-1.84	0.745	0.915	-7.9
longan shell	NF-3.12	0.829	-1.50	0.775	0.925	-6.6
white beech mushroom	NF-3.16	0.830	-1.45	0.778	0.921	-7.2
oil bran	NF-3.70	0.838	-1.78	0.779	0.925	-5.6
apricot flowers	NF-4.07	0.852	-1.36	0.801	0.934	-6.6
radish leaves	NF-4.25	0.840	-1.53	0.802	0.923	-6.2
corn stigmas	NF-4.54	0.841	-6.08	0.804	0.932	-7.7
winter melon peel	NF-4.60	0.850	-3.92	0.807	0.929	-6.7
durian peel	NF-4.75	0.858	-1.74	0.810	0.937	-6.0
willow leaves	NF-4.80	0.859	-3.86	0.811	0.940	-8.2
alfalfa	NF-4.84	0.863	-2.42	0.806	0.939	-10.4
banana peel	NF-4.88	0.854	-2.50	0.812	0.940	-7.8
radish peel	NF-5.35	0.850	-1.16	0.805	0.927	-8.5
leek moss	NF-5.60	0.854	-2.32	0.801	0.930	-6.3
dandelion leaves	NF-5.80	0.849	-1.90	0.799	0.932	-6.1
long bean	NF-5.89	0.844	-1.38	0.791	0.927	-8.4
sweet potato stems	NF-6.09	0.841	-1.59	0.789	0.928	-6.5
orange peel	NF-6.51	0.839	-2.50	0.786	0.928	-6.8
soybean curb residue	NF-6.61	0.833	-2.12	0.783	0.931	-6.0
firmiana simplex flowers	NF-6.64	0.830	-2.20	0.769	0.927	-10.6
sweet potato leaves	NF-6.67	0.830	-2.05	0.765	0.925	-8.4
wheat stalk	NF-8.02	0.831	-1.87	0.745	0.917	-6.1
solidago	NF-8.37	0.843	-2.16	0.755	0.922	-7.0
pepper leaves	NF-9.91	0.810	-1.55	0.745	0.930	-12.5
-	Pt/C	0.830	-1.75	0.805	0.963	-6.6

[a)]Peak potential; [b)]Peak current density; [c)]Half-wave potential; [d)]Onset potential; [e)]Diffusion-limited current density.

Table S4 Comparison of electrocatalytic performances in terms of ORR half-wave potential (0.1 M KOH) & OER potential at 10 mA cm^{-2} (1 M KOH) and ZAB performance between this work and other related reports.

references	$E_{half\text{-}wave}$ [V][a)]	$E_{j=10}$ [V][b)]	P_{ZAB} [mW cm^{-2}][c)]	S_{ZAB} [h][d)]
This work	0.806	1.41	116	88 h at 5 mA cm^{-2}
1	0.8153	1.5983	97	66 h at 5 mA cm^{-2}
2	0.84	-	67	60 h at 5 mA cm^{-2}
3	0.83	-	115	-
4	0.85	1.6	175	50 h at 10 mA cm^{-2}
5	0.80	1.54	135	136 h at 10 mA cm^{-2}
6	0.79	-	152	60 h at 2 mA cm^{-2}
7	0.817	1.58	105	40 h at 5 mA cm^{-2}
8	0.85	1.57	151	55 h at 5 mA cm^{-2}
9	0.85	1.68	115	78 h at 10 mA cm^{-2}
10	0.790	1.542	-	80 h at 25 mA cm^{-2}
11	0.81	1.51	81	160 h at 10 mA cm^{-2}
12	0.90 V	-	125	60 h at 5 mA cm^{-2}

[a)]ORR half-wave potential; [b)]OER potential at 10 mA cm^{-2}. [c)]Peak power density of ZAB with catalyst. [d)]Long-term stability of ZAB with catalyst.

References

1. T. Li, Y. Lu, S. Zhao, Z.-D. Gao, Y.-Y. Song, *J. Mater. Chem. A*, 2018, **6,** 3730.
2. L. Wang, K. Liang, L. Deng, Y.-N. Liu, *Appl. Catal. B,* 2019, **246,** 89.
3. F. Li, Y. Yin, C. Zhang, W. Li, K. Maliutina, Q. Zhang, Q. Wu, C. He, Y. Zhang, M. Yang, L. Fan, *Appl. Catal. B,* 2020, **263,** 118297.
4. K. He, J. Zaia, X. Liu, Y. Zhu, A. Iqbal, T. T. Tsega, Y. Zhang, N. Ali, X. Qian, *Appl. Catal. B,* 2020, **265,** 118594.
5. F. Meng, H. Zhong, D. Bao, J. Yan, X. Zhang, *J. Am. Chem. Soc.,* 2016, **138,** 10226.
6. C. Tang, B. Wang, H.-F. Wang, Q. Zhang, *Adv. Mater.,* 2017, **29,** 1703185.
7. M. Zhang, Q. Dai, H. Zheng, M. Chen, L. Dai, *Adv. Mater.,* 2018, **30,** 1705431.
8. Z. Pei, H.Li, Y. Huang, Q. Xue, Y. Huang, M. Zhu, Z. Wang, C. Zhi, *Energy Environ. Sci.,* 2017, **10,** 742.
9. Q. Wang, Y. Ji, Y. Lei, Y. Wang, Y. Wang, Y. Li, S. Wang, *ACS Energy Lett.,* 2018, **3,** 1183.
10. Q. Wang, L. Shang, R. Shi, X. Zhang, Y. Zhao, G. I. N. Waterhouse, L.-Z. Wu, C.-H. Tung, T. Zhang, *Adv. Energy Mater.,* 2017, **7,** 1700467.
11. X. F. Lu, S. L. Zhang, E. Shangguan, P. Zhang, S. Gao, X. W. (David) Lou, *Adv. Sci.*, 2020, **7,** 2001178.
12. L.-L. Ma, W.-J. Liu, X. Hu, P. K.S. Lam, J. R. Zeng, H.-Q. Yu, *Chem. Eng. J.,* 2020*,* **400,** 125969.